

## 数值孔径对飞秒激光角膜切削的影响

吕海军<sup>1</sup>, 王雨<sup>1</sup>, 李华明<sup>1</sup>, 张卓宇<sup>1</sup>, 赵新恒<sup>2\*\*</sup>, 吕晓华<sup>1\*</sup>, 刘秀丽<sup>1</sup>, 曾绍群<sup>1</sup><sup>1</sup>华中科技大学武汉光电国家研究中心, 高端生物医学成像重大科技基础设施, 生物医学光子学教育部重点实验室, Britton Chance 生物医学光子学研究中心, 湖北 武汉 430074;<sup>2</sup>天津市眼科医院, 南开大学附属眼科医院, 天津医科大学眼科临床学院, 南开大学眼科学研究院, 天津 300020

**摘要** 飞秒激光得益于其精准、微创等优势被广泛应用于屈光疾病的治疗。在飞秒激光屈光手术中, 光学系统的数值孔径是影响手术效果的重要参数。本研究旨在探讨数值孔径对飞秒激光角膜基质切削质量的影响规律, 以帮助临床医生更好地选择合适的手术参数。选用 0.16、0.30、0.80 三种数值孔径进行离体动物角膜的飞秒激光切削实验, 并通过气泡尺寸与凋亡细胞比例评估激光切削质量与基质细胞损伤程度。实验结果显示: 气泡体积随着数值孔径的增大而减小, 高数值孔径下切割更易实现基质层的分离; 上述三种数值孔径下的基质细胞损伤比例分别为 9.4%、4.9% 和 1.0%, 基质细胞的损伤比例随着数值孔径的增大而明显下降。因此, 增大数值孔径有助于提高飞秒激光角膜基质切削的安全性。

**关键词** 激光技术; 飞秒激光; 角膜; 数值孔径; 气泡; 细胞损伤

中图分类号 R778

文献标志码 A

DOI: 10.3788/CJL231537

## 1 引言

角膜激光屈光手术是通过激光对角膜组织进行消融或者切削来改变角膜曲率和厚度, 从而实现屈光矫正的方法<sup>[1-4]</sup>。其中, 飞秒激光角膜切削技术作为一种精确、微创、可控制的手术方式, 在眼科屈光手术中得到了广泛应用<sup>[5-8]</sup>。

在飞秒屈光手术中, 激光聚焦于角膜基质内部产生等离子体, 等离子体爆破生成的冲击波诱导组织断裂<sup>[9]</sup>, 同时产生的空化气泡进一步撕裂角膜层间结构, 实现角膜切削<sup>[5,10]</sup>。空化气泡的体积取决于聚焦光斑的尺寸与注入脉冲能量的大小, 大的光学数值孔径 (NA) 与低的脉冲能量可以获得更小的聚焦光斑。Lubatschowski<sup>[11]</sup>认为: 切割区域由激光焦斑尺寸限定; 相比于低数值孔径切削, 使用高数值孔径、低脉冲能量开展屈光手术可以产生更加柔和的气泡层, 有助于皮瓣分离。

在激光切削过程中, 飞秒激光会对周围组织造成一定损伤<sup>[12-16]</sup>, 而且不同的数值孔径所需的激光脉冲能量有所不同: 低数值孔径需要更高的能量才能达到角膜切削所需的能量密度阈值, 而更高的能量则伴随着更大的爆破区域以及更严重的热影响区; 高数值孔径允许使用更低的能量进行切削, 爆破区域小且对周围组织的热损伤小<sup>[5]</sup>。2009年, de Medeiros等<sup>[17]</sup>分析了不同飞秒激光能量水平对角膜基质细胞死亡和炎症

的影响, 结果表明: 更高的飞秒激光能量水平不仅会导致更多的细胞死亡, 还会导致更大的角膜炎症细胞浸润。2013年, Phillips等<sup>[18]</sup>分析了激光能量对角膜内皮细胞存活率的影响, 实验表明: 脉冲能量越低, 内皮细胞的存活率越高, 激光手术的安全性越高。因此, 低能量有利于降低周围组织细胞的损伤。提高数值孔径可以有效降低切削能量。

2014年, Riau等<sup>[19]</sup>采用两款不同数值孔径的手术设备进行了角膜切削实验, 并进一步分析了微秒和纳秒脉冲激光能量下的皮瓣黏附强度与术后愈合反应等。结果表明: 高数值孔径下, 纳秒脉冲激光能量对角膜细胞的损伤更小, 伤口愈合反应更小。在飞秒屈光手术中, 单脉冲能量越低, 角膜内细胞的损伤越小。

目前, 从气泡形态、剥离难易程度、基质细胞损伤等方面评估飞秒激光切削质量, 研究不同数值孔径对飞秒激光切削影响的相关报道较少。鉴于此, 笔者搭建了一台可调节数值孔径的飞秒激光角膜切削系统, 旨在研究飞秒屈光手术过程中不同数值孔径下的气泡形态差异、层瓣分离的难易程度以及基质细胞损伤等情况, 为飞秒屈光手术系统的优化提供实验支撑。

## 2 原理与设计

## 2.1 基本原理

飞秒脉冲激光具有极高的峰值能量, 激光焦点处的光功率密度可达  $10^{11}$  W/cm<sup>2</sup>, 在这种情况下会产生

收稿日期: 2023-12-16; 修回日期: 2024-02-02; 录用日期: 2024-02-05; 网络首发日期: 2024-02-25

通信作者: \*xhly@hust.edu.cn; \*\*zhaoxinheng@foxmail.com

“光击穿”效应(LIOB)<sup>[5]</sup>。如图 1(a)所示,高密度光子引起非线性多光子吸收,导致一些组织分子电离产生自由电子,即种子电子<sup>[5]</sup>。产生的种子电子不断吸收光子能量,获得足够高的动能,进而通过碰撞电离产生更多的自由电子<sup>[20]</sup>。自由电子密度急剧增大,在激光焦点处产生“等离子态物质”,即等离子体<sup>[20]</sup>。等离子体爆破

生成的冲击波诱导组织断裂<sup>[10]</sup>。同时,等离子体产生后,组织内部因高温与高压而不断膨胀,导致焦点处的组织发生破坏,组织中的液体蒸发,产生水蒸气、H<sub>2</sub>、O<sub>2</sub>、甲烷和乙烷等气体,从而在激光焦点处形成空化气泡<sup>[10]</sup>,如图 1(b)所示。产生的气体将周围组织向外推离,撕裂基质层,实现切削<sup>[5,21-23]</sup>,如图 1(c)所示。

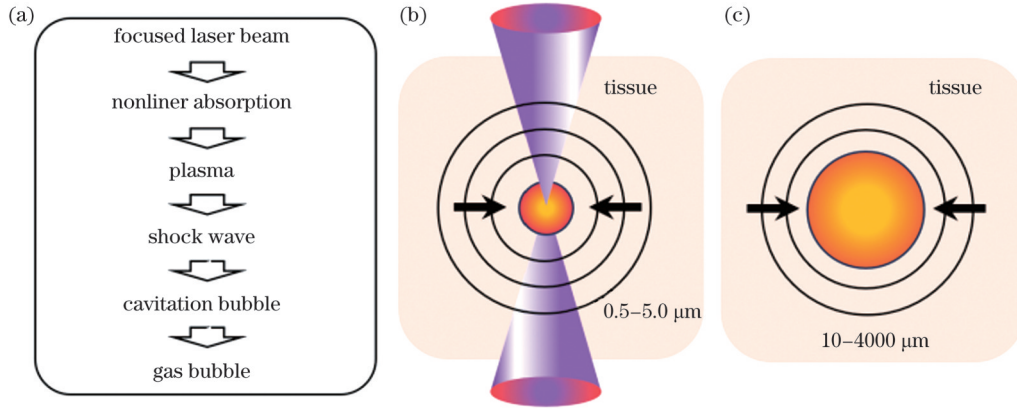


图 1 短脉冲激光在组织中的作用。(a)效应顺序和诱发事件;(b)等离子体尺寸范围和压力波模式;(c)空化气泡尺寸的范围(与脉冲能量相关)<sup>[5]</sup>

Fig. 1 Short pulse laser effects in tissue. (a) Sequence of effects and induced events; (b) plasma size range and pressure wave pattern; (c) range of cavitation bubble dimensions (pulse energy-dependent)<sup>[5]</sup>

飞秒激光诱导组织烧蚀的剧烈程度取决于焦点处脉冲激光的峰值能量密度。峰值功率体密度的表达式<sup>[24]</sup>为

$$P_{\text{peak}} = \frac{E}{\tau \cdot V}, \quad (1)$$

式中:  $P_{\text{peak}}$  为峰值功率体密度;  $E$  为激光单脉冲能量;  $\tau$  为激光脉冲宽度;  $V$  为聚焦光斑体积。聚焦光斑体积与数值孔径的关系为

$$V \approx \frac{\pi \lambda^3}{15 \cdot (NA)^4}, \quad (2)$$

式中:  $\lambda$  为激光波长;  $NA$  为数值孔径值。由式(2)可以看出,聚焦体积  $V$  与数值孔径  $NA$  的四次方成反比。数值孔径越大,聚焦光斑的体积越小,诱导产生的空化气泡越小。

将式(2)代入式(1)可得峰值功率体密度与数值孔径、单脉冲能量的关系为

$$P_{\text{peak}} \approx \frac{15 \cdot E \cdot (NA)^4}{\pi \cdot \tau \cdot \lambda^3}. \quad (3)$$

由式(3)可以看出,在峰值功率体密度  $P_{\text{peak}}$  一定的情况下,数值孔径越大,单脉冲能量  $E$  越小。因此,通过提高光学系统的数值孔径,可以有效降低注入单脉冲能量  $E$ ,从而降低细胞损伤,提高手术的安全性,有利于降低术后并发症的发生概率。

## 2.2 飞秒角膜切削系统设计

搭建的数值孔径可调的飞秒激光角膜切削系统的光路如图 2 所示。激光扩束器(BE)采用伽利略结构对光束进行 4 倍扩束,最大光束直径为 12 mm。半

玻片(HWP)与偏振分光棱镜组合使用,旋转半波片可以改变偏振光透过分光棱镜(PBS)的比例,实现能量调节。可变孔径光阑(VH)用于调节光束直径  $D$ 。由数值孔径计算公式  $NA \approx D/(2f)$  可知,在物镜焦距  $f$  不变的情况下,通过改变入射物镜光束的尺寸  $D$ ,可以调节数值孔径。采样镜(SM)分离的 1% 能量入射至功率计(PM)。在激光加工过程中,可以通过功率计实时监测加工能量。振镜(GS)为扫描器件,4f 中继系统将振镜中心成像到物镜(OBJ, Olympus, LUMPLFLN40XW)入瞳中心,防止边缘视场光束被截。系统中采用的是截止波长为 850 nm 的长通短反二向色镜(DM),1035 nm 红外激光透过二向色镜进行加工,成像可见光被二向色镜反射并被管镜(TL)收集于成像相机(Cam)。为了防止反射红外激光对成像造成干扰,在成像光路中添加低通滤光片(SPF),滤除红外光。实验所用物镜的最大扫描视场直径仅为 0.36 mm,因此,实验中采用扫描振镜(GS)与三轴平移台配合进行马赛克拼接实现大视场扫描,如图 3 所示。通过调节入射光束的直径与马赛克拼接方案,可以实现不同数值孔径下的大视场角膜切削。

## 2.3 飞秒制瓣实验

飞秒激光角膜切削实验使用新鲜的离体猪眼球进行。所用猪眼球来自当地屠宰场,并于取样后 6 h 内冷链运输至实验室进行相关实验。实验过程中采用冰盒保存未使用的猪眼球,所有猪眼球均在 12 h 内使用。实验前,修剪猪眼球周围多余的赘肉与过长的

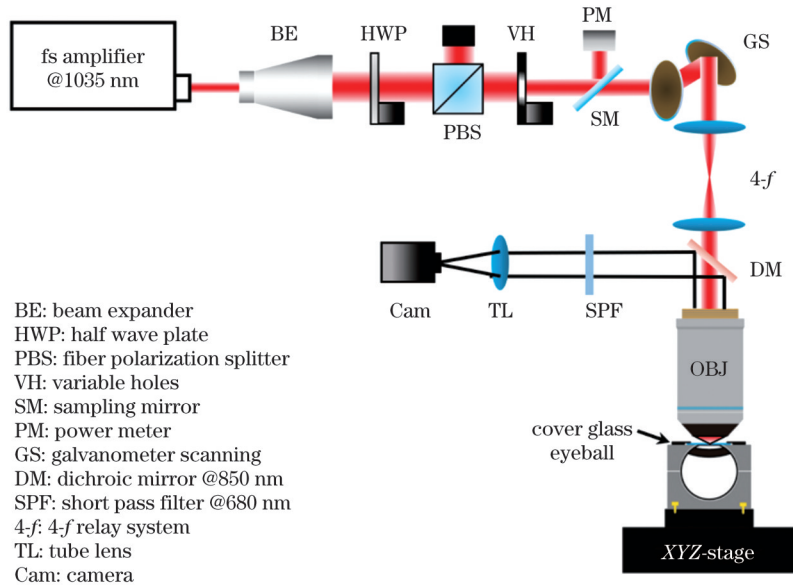


图2 飞秒激光角膜切削系统原理图

Fig. 2 Schematic diagram of femtosecond laser corneal ablation system

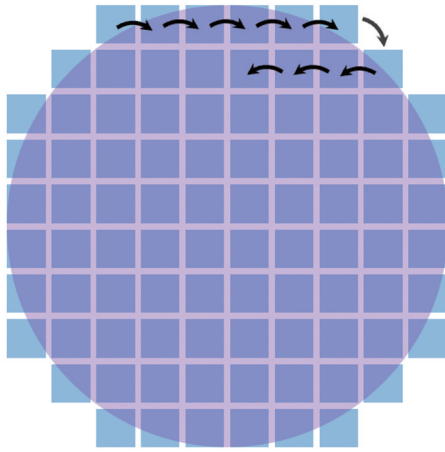


图3 马赛克拼接扫描轨迹

Fig. 3 Mosaic stitching scanning trajectory

视神经,将处理好的猪眼球置于自制的圆形容容器内,并用盖玻片将猪眼角膜压平固定。将放置猪眼球的容器固定于精密三维平移台上,以便实现样品的移动控制。

调节入射光束直径,分别在 0.16、0.30、0.80 数值孔径下,使用飞秒激光制作了角膜瓣,制作流程如图 4 所示,其中下图为俯视图,上图为黑色虚线处的剖面图。在基质层 200  $\mu\text{m}$  深度处切削一个直径为 8.0 mm 的圆形分离面,如图 4(a) 灰色区域所示,然后沿着圆周切割一个 270° 柱面侧切口,如图 4(a) 灰色虚线所示,从而在角膜上制作出角膜瓣。在不同数值孔径制瓣实验中,扫描点间距设定为光斑直径的 1.5 倍,单脉冲能量分别设定为 1005、235、26 nJ。不同数值孔径下设定的能量通过基于辉光强度的光击穿阈值测量系统测得<sup>[25]</sup>。

制瓣手术完成后,迅速将猪眼球放置于显微镜

(Axio Zoom. V16, Zeiss) 下观察气泡形态并进行记录;然后使用分离匙将飞秒激光切削的角膜瓣掀开,将角膜瓣与基质层分离,如图 4(b) 所示,记录分离的流畅程度。

#### 2.4 基质细胞损伤实验

细胞损伤实验参考 TUNEL<sup>[19]</sup> (TdT-mediated dUTP nick end labeling, C1088, Beyotime) 染色方法进行。选用成年新西兰大白兔 (2~2.5 kg) 进行实验,先用 1 mL 盐酸替来他明盐酸唑拉西洋注射液 (Zoletil<sup>®</sup> 50, Virbac) 对其进行麻醉处理,而后通过静脉空气注射将其处死,将兔眼球取下并固定于特定的夹持器内,采用飞秒激光角膜切削系统在 0.16、0.30、0.80 三组数值孔径下开展制瓣手术。

基质细胞损伤实验过程如下: 1) 将通过飞秒激光制瓣切削获得的兔眼球放在角膜活性中期保存液 (DX 液) 中,并置于 4 °C 环境下培育 6 h,使受损的角膜基质细胞进入凋亡过程; 2) 将兔眼球取出,放置于 4% 多聚甲醛 (PFA) 溶液中预固定 2 h; 3) 沿虹膜边缘裁剪兔眼角膜,将取下的角膜组织放置于 PFA 和冰醋酸按 4:1 体积比配制而成的混合液中固定 14 h; 4) 角膜组织经过乙醇梯度脱水后进行石蜡包埋,石蜡包埋的样本采用切片 (RM2255, Leica) 制成 6  $\mu\text{m}$  厚的组织切片; 5) 经脱蜡和复水后,使用 DAPI (4, 6-diamidino-2-phenylindole, D9542, Sigma-Aldrich) 和 TUNEL 对角膜切片进行双染。DAPI 能够对细胞核进行染色,用于定位角膜基质内的基质细胞并统计基质细胞的数目; TUNEL 能够标记凋亡的基质细胞,用于统计飞秒激光手术中损伤细胞的数目。在荧光显微镜 (Axio Zoom. V16, Zeiss) 下对细胞进行成像并统计凋亡细胞的数目。

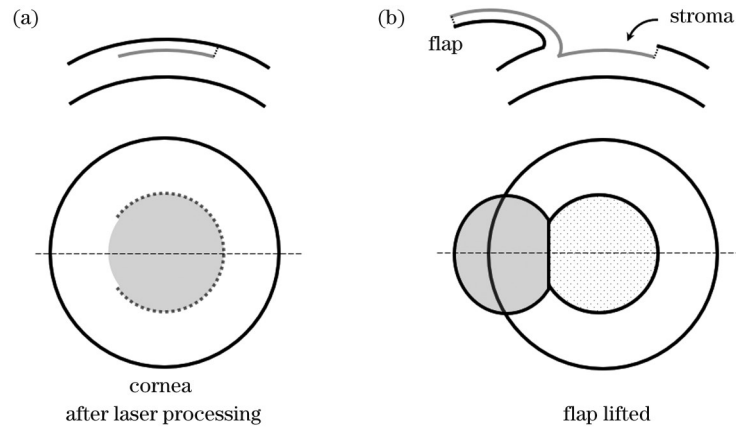


图 4 飞秒激光制作角膜瓣示意图。(a)飞秒激光切削区域,包括基底切割(灰色)与侧切(虚线);(b)将角膜瓣掀开,暴露基质层  
Fig. 4 Diagrams of corneal flap prepared by femtosecond laser. (a) Femtosecond laser ablation area, including the basal cut (gray) and the side cut (dashed); (b) lifting the corneal flap to expose stromal layer

### 3 实验与结果

#### 3.1 气泡形态与切面质量分析

0.16、0.30、0.80 三种数值孔径下的飞秒激光制瓣结果如图 5 所示。图 5(a)~(c)展示了不同数值孔径下切削区域形成的均匀的气泡层。由图 5(d)~(f)可以看出,随着数值孔径增大,气泡体积逐渐减小,气泡更加致密。另外可以看出单个气泡并非圆形,这是由于在飞秒激光切削过程中,相邻的空化气泡相互融合形成了一个更大的气泡,而融合过程是随机的,因此合成的大气泡形态不规则。

对图 5(a)~(c)中的气泡尺寸进行统计,分别绘制每个数值孔径下气泡尺寸的箱线图和散点图,箱线图如图 6 所示。可以看出,随着数值孔径增大,气泡尺寸逐渐减小。这可由式(2)进行解释,随着数值孔径增大,光斑的聚焦体积逐渐减小,光斑聚焦体积越小,诱导产生的气泡的体积越小。

使用分离匙将角膜瓣掀开,记录角膜瓣分离的难易程度。结果显示,高数值孔径下制备的角膜瓣更易分离。在高数值孔径下,飞秒激光诱导产生的气泡更小,致密的气泡层可以更好地分离基质层间的间隙,层间粘连更少,因此角膜瓣分离更加容易。

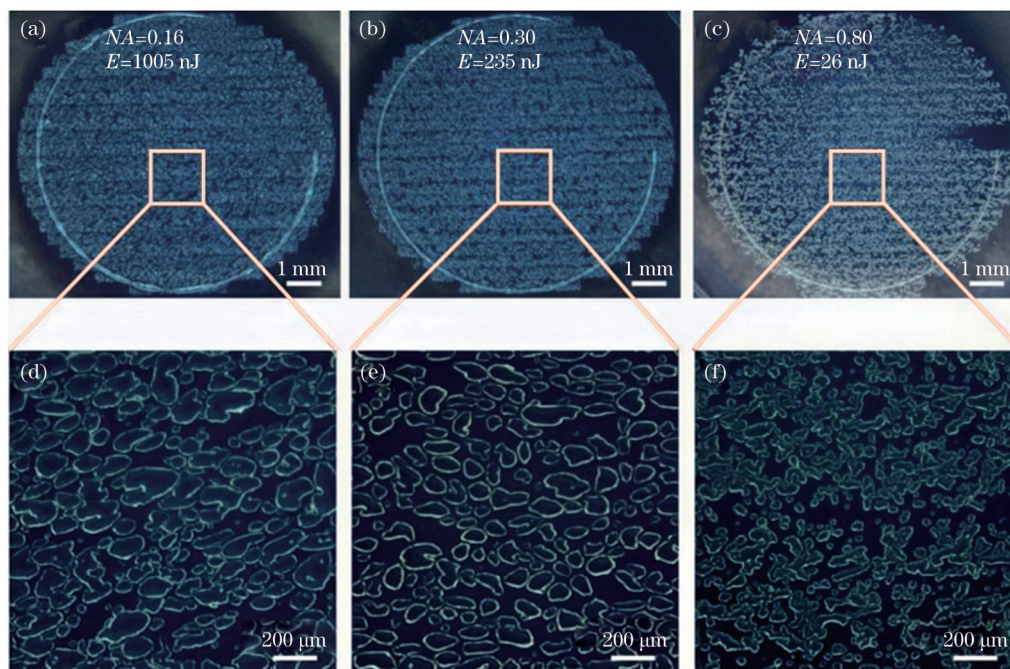


图 5 不同数值孔径下的角膜制瓣结果。(a)~(c) 0.16、0.30、0.80 数值孔径下,飞秒激光切削后的气泡层;(d)~(f)对应数值孔径下气泡层的局部放大图

Fig. 5 Results of corneal flap creation under different numerical aperture values. (a)~(c) Bubble layer after femtosecond laser ablation under numerical aperture values of 0.16, 0.30, and 0.80; (d)~(f) local magnification images of the bubble layer under corresponding numerical aperture values

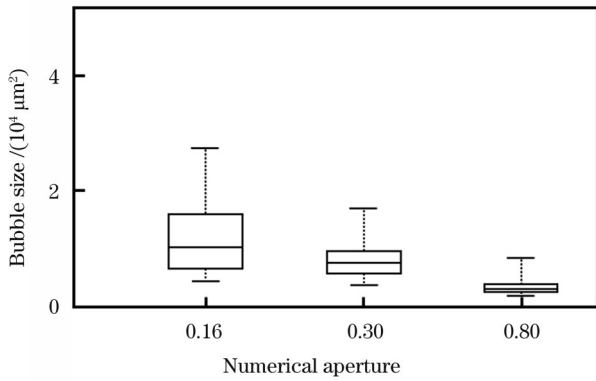


图 6 气泡尺寸统计结果

Fig. 6 Statistical bubble size

### 3.2 细胞损伤分析

针对离体兔眼角膜研究 0.16、0.30、0.80 三种数值孔径下飞秒激光对基质细胞损伤的影响。分别使用

DAPI 和 TUNEL 对角膜切片进行染色,染色结果如图 7(a)~(c)所示,其中:红色为 TUNEL 染色的凋亡细胞,采用橙色箭头指示;蓝色为 DAPI 染色的正常细胞,用于统计细胞总数。由图 7(a)~(c)可以看出,采用更低的数值孔径进行角膜切削时,在角膜基质内有一个条带区域发生了明显的细胞凋亡,而且随着数值孔径增大,凋亡细胞的数量明显减少。

针对每一个数值孔径,统计了 8 个  $636 \mu\text{m} \times 636 \mu\text{m}$  视场范围角膜基质细胞的损伤比例,如图 7(d)所示。数值孔径为 0.16、0.30 和 0.80 时,基质细胞的损伤比例分别为 9.4%、4.9% 和 1.0%。可以看出,随着数值孔径增大,出现基质损伤的细胞占比明显降低。这是由于高的数值孔径所用的激光单脉冲能量更低,聚焦光斑更小,爆破区域更小,对周围组织的损伤更小。因此,增大数值孔径有利于降低基质细胞的损伤程度。

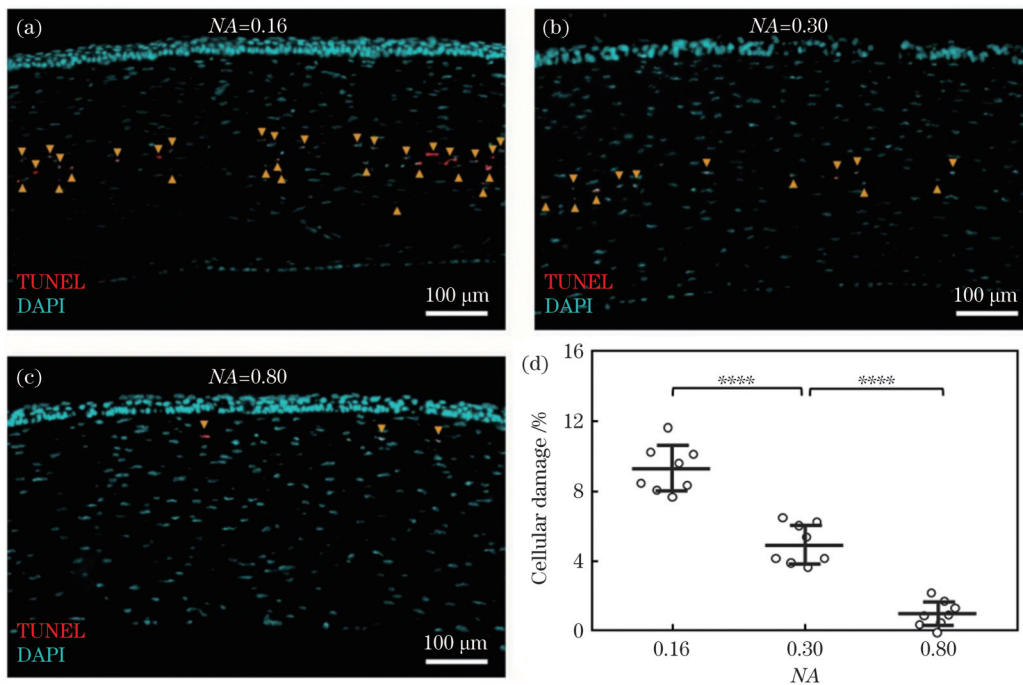


图 7 飞秒激光角膜基质切削过程中的细胞损伤结果。(a)数值孔径为 0.16;(b)数值孔径为 0.30;(c)数值孔径为 0.80;(d)细胞损伤比例统计结果,图中误差棒为均值±误差,样本数  $n=10$ ,\*\*\*\*表示  $P<0.0001$

Fig. 7 Cell damage in femtosecond laser corneal stromal ablation. (a) Numerical aperture is 0.16; (b) numerical aperture is 0.30; (c) numerical aperture is 0.80; (d) statistics of stromal cell damage proportion, where the error bars in the figure are mean  $\pm$  standard error, sample quantity  $n=10$ , \*\*\*\* denotes  $P<0.0001$

## 4 结 论

研究了不同数值孔径下飞秒激光对角膜切削的影响,分析了不同数值孔径飞秒激光作用下气泡的形态差异,比较了切削基质层分离的难易程度,统计了细胞的损伤比例。实验结果表明,采用飞秒激光切削角膜时,数值孔径越大,产生的气泡越小,气泡层越致密,角膜瓣越易分离,基质细胞损伤的程度越低。大的数值孔径有利于飞秒激光角膜切削。

## 参 考 文 献

- [1] Yan Q, Han B, Ma Z C. Femtosecond laser-assisted ophthalmic surgery: from laser fundamentals to clinical applications[J]. Micromachines, 2022, 13(10): 1653.
- [2] 魏升升, 李勇, 李晶, 等. 飞秒激光在眼科圆锥角膜治疗中的新进展[J]. 中国激光, 2022, 49(15): 1507103.  
Wei S S, Li Y, Li J, et al. Recent progress in femtosecond laser in treatment of ophthalmic keratoconus[J]. Chinese Journal of Lasers, 2022, 49(15): 1507103.
- [3] Gadhvi K A, Romano V, Fernández-Vega Cueto L, et al. Femtosecond laser-assisted deep anterior lamellar keratoplasty for keratoconus: multi-surgeon results[J]. American Journal of

- Ophthalmology, 2020, 220: 191-202.
- [4] 钟文倩, 陈仪乐, 李金瑛. 飞秒激光在眼科手术中的应用[J]. 罕少疾病杂志, 2022, 29(5): 107-109.  
Zhong W Q, Chen Y L, Li J Y. Application of femtosecond laser in ophthalmic surgery[J]. Journal of Rare and Uncommon Diseases, 2022, 29(5): 107-109.
- [5] Latz C, Asshauer T, Rathjen C, et al. Femtosecond-laser assisted surgery of the eye: overview and impact of the low-energy concept [J]. Micromachines, 2021, 12(2): 122.
- [6] Sioufi K, Zheleznyak L, MacRae S, et al. Femtosecond lasers in cornea & refractive surgery[J]. Experimental Eye Research, 2021, 205: 108477.
- [7] 侯蕊, 赵智慧, 赵越. 准分子激光治疗机角膜切削深度检测方法研究[J]. 光学技术, 2022, 48(3): 323-327.  
Hou R, Zhao Z H, Zhao Y. Research on the testing method of the corneal ablation depth of excimer laser corneal ametropia cure system[J]. Optical Technique, 2022, 48(3): 323-327.
- [8] 田轩, 田文龙, 李乾, 等. 基于宽带高反镜色散补偿的高功率克尔透镜锁模飞秒激光器[J]. 中国激光, 2023, 50(7): 0701001.  
Tian X, Tian W L, Li Q, et al. High power Kerr-lens mode-locked femtosecond laser with broadband highly reflective mirrors compensating dispersion[J]. Chinese Journal of Lasers, 2023, 50(7): 0701001.
- [9] Vogel A, Noack J, Hüttman G, et al. Mechanisms of femtosecond laser nanosurgery of cells and tissues[J]. Applied Physics B, 2005, 81(8): 1015-1047.
- [10] Heisterkamp A, Ripken T, Lubatschowski H, et al. Intrastromal cutting effects in rabbit cornea using femtosecond laser pulses[J]. Proceedings of SPIE, 2000, 4161: 52-60.
- [11] Lubatschowski H. Overview of commercially available femtosecond lasers in refractive surgery[J]. Journal of Refractive Surgery, 2008, 24(1): S102-S107.
- [12] Binder P S. One thousand consecutive IntraLase laser *in situ* keratomileusis flaps[J]. Journal of Cataract and Refractive Surgery, 2006, 32(6): 962-969.
- [13] Haft P, Yoo S H, Kymionis G D, et al. Complications of LASIK flaps made by the IntraLase 15- and 30-kHz femtosecond lasers[J]. Journal of Refractive Surgery, 2009, 25(11): 979-984.
- [14] Mayer W J, Klaproth O K, Ostovic M, et al. Cell death and ultrastructural morphology of femtosecond laser-assisted anterior capsulotomy[J]. Investigative Ophthalmology & Visual Science, 2014, 55(2): 893-898.
- [15] Schultz T, Joachim S C, Stellbogen M, et al. Prostaglandin release during femtosecond laser-assisted cataract surgery: main inducer[J]. Journal of Refractive Surgery, 2015, 31(2): 78-81.
- [16] Schwarzenbacher L, Schartmüller D, Leydolt C, et al. Intraindividual comparison of cytokine and prostaglandin levels with and without low-energy, high-frequency femtosecond laser cataract pretreatment after single-dose topical NSAID application [J]. Journal of Cataract and Refractive Surgery, 2020, 46(8): 1086-1091.
- [17] de Medeiros F W, Kaur H, Agrawal V, et al. Effect of femtosecond laser energy level on corneal stromal cell death and inflammation[J]. Journal of Refractive Surgery, 2009, 25(10): 869-874.
- [18] Phillips P M, Phillips L J, Saad H A, et al. "UlthraThin" DSAEK tissue prepared with a low-pulse energy, high-frequency femtosecond laser[J]. Cornea, 2013, 32(1): 81-86.
- [19] Riau A K, Liu Y C, Lwin N C, et al. Comparative study of nJ- and  $\mu$ J-energy level femtosecond lasers: evaluation of flap adhesion strength, stromal bed quality, and tissue responses[J]. Investigative Ophthalmology & Visual Science, 2014, 55(5): 3186-3194.
- [20] Kaschke M, Donnerhacke K H, Rill M S. Optical devices in ophthalmology and optometry: technology, design principles and clinical applications[M]. Weinheim: Wiley, 2014.
- [21] Lengert L, Lohmann H, Johannsmeier S, et al. Optoacoustic tones generated by nanosecond laser pulses can cover the entire human hearing range[J]. Journal of Biophotonics, 2022, 15(11): e202200161.
- [22] Vogel A, Busch S, Jungnickel K, et al. Mechanisms of intraocular photodisruption with picosecond and nanosecond laser pulses[J]. Lasers in Surgery and Medicine, 1994, 15(1): 32-43.
- [23] Vogel A, Lauterborn W. Acoustic transient generation by laser-produced cavitation bubbles near solid boundaries[J]. The Journal of the Acoustical Society of America, 1988, 84(2): 719-731.
- [24] 周炳琨, 高以智, 陈倜嵘, 等. 激光原理[M]. 6版. 北京: 国防工业出版社, 2009.  
Zhou B K, Gao Y Z, Chen T R. Laser principle[M]. 6th ed. Beijing: National Defense Industry Press, 2009.
- [25] Sun H, Han M, Niemz M H, et al. Femtosecond laser corneal ablation threshold: dependence on tissue depth and laser pulse width [J]. Lasers in Surgery and Medicine, 2007, 39(8): 654-658.

## Effect of Numerical Aperture on Femtosecond Laser Corneal Ablation

Lü Haijun<sup>1</sup>, Wang Yu<sup>1</sup>, Li Huaming<sup>1</sup>, Zhang Zhuoyu<sup>1</sup>, Zhao Xinheng<sup>2\*\*</sup>, Lü Xiaohua<sup>1\*</sup>,  
Liu Xiuli<sup>1</sup>, Zeng Shaoqun<sup>1</sup>

<sup>1</sup>*Britton Chance Center for Biomedical Photonics, MOE Key Laboratory for Biomedical Photonics, Advanced Biomedical Imaging Facility, Wuhan National Laboratory for Optoelectronics, Huazhong University of Science and Technology, Wuhan 430074, Hubei, China;*

<sup>2</sup>*Tianjin Eye Hospital, Affiliated Eye Hospital of Nankai University, Clinical School of Ophthalmology, Tianjin Medical University, Institute of Ophthalmology, Nankai University, Tianjin 300020, China*

### Abstract

**Objective** Corneal laser refractive surgery is a method for correcting vision using lasers to reshape the cornea and change its curvature and thickness. Femtosecond laser corneal cutting is widely used in ophthalmic refractive surgery as a precise, minimally invasive, and controllable surgical technique. In femtosecond laser refractive surgery, the numerical aperture of the optical system determines the focal spot size and required single-pulse energy, which are critical parameters that influence the corneal cutting quality. In this study, we built a femtosecond laser surgery system with an adjustable numerical aperture. We investigated the effect of numerical aperture on cutting quality in the corneal stroma by analyzing the differences in bubble morphology, smoothness of flap separation, and proportion of damaged stromal cells. This study aimed to assist clinicians in selecting the appropriate surgical

parameters more effectively.

**Methods** Freshly enucleated pig eyeballs and New Zealand white rabbits were selected as experimental subjects. By adjusting the diameter of the incident beam, corneal flaps were formed on the pig eyeballs using a femtosecond laser with numerical aperture values of 0.16, 0.30, and 0.80. The morphology of the bubbles after cutting was recorded, and the smoothness of the separation was observed when the corneal flaps were lifted. Cell damage experiments were conducted by cutting New Zealand white rabbit eyeballs with a femtosecond laser at numerical aperture values of 0.16, 0.30, and 0.80. After creating the flap with the femtosecond laser, the rabbit eyeballs were placed in corneal active medium (DX solution) and incubated at 4 °C for 6 h to induce apoptosis in the damaged corneal stromal cells. Subsequently, the rabbit eyeballs were removed and prefixed in a 4% paraformaldehyde (PFA) solution for 2 h. After dewaxing and rehydration, the corneal sections were double-stained with DAPI (4,6-diamidino-2-phenylindole, D9542, Sigma-Aldrich) and TUNEL (TdT-mediated dUTP nick end labeling, C1088, Beyotime). Finally, the apoptotic cell counts were determined by imaging the sections under a fluorescence microscope.

**Results and Discussions** Under the three different numerical aperture values (0.16, 0.30, and 0.80), as the numerical aperture increases, the volume of the bubbles decreases gradually, and the density of the bubble layer increases (Figs. 5 and 6). This is mainly attributed to the decreasing volume of the focal spot with an increasing numerical aperture, which decreases cavitation bubbles. Corneal flaps formed at a higher numerical aperture are easier to separate. This is primarily because smaller cavitation bubbles result in a denser bubble layers, which facilitates the separation of the interlamellar space with less adhesions between the tissue layers. In the cell damage experiment, as numerical aperture increases, the number of apoptotic cells decreases significantly, as shown in Fig. 7. This is attributed to the decreased single-pulse energy and decreased focal spot size associated with an increase in numerical aperture, which results in smaller photodisruption zones and reduced damage to the surrounding tissues. Therefore, increasing the numerical aperture is beneficial for reducing the extent of stromal cell damage.

**Conclusions** The effects of femtosecond laser corneal cutting for different numerical aperture values were investigated experimentally. The morphological differences in cavitation bubbles induced by a femtosecond laser at different numerical aperture values were analyzed, and the ease of separation of the lamellar layers and the extent of cell damage were compared. The results of the experiment show that during femtosecond laser corneal cutting, a higher numerical aperture yields smaller bubbles, denser bubble layers, easier separation of corneal flaps, and lower levels of damage to stromal cells. Therefore, a higher numerical aperture is beneficial in femtosecond laser refractive surgery. Overall, this study provides valuable insights into the effects of numerical aperture on femtosecond laser corneal cutting and highlights the importance of optimizing the numerical aperture to achieve improved treatment outcomes in corneal procedures.

**Key words** laser technique; femtosecond laser; cornea; numerical aperture; bubble; cell damage